Extension to E93-021: The Charged Pion Form Factor

(December 13, 2000)

E.J. Brash, G.M. Huber (Co-spokesman), A. Kozlov, G.J. Lolos, Z. Papandreou
Department of Physics, University of Regina, Regina, SK, Canada

D. Abbott, R. Carlini, R. Ent, K. Garrow, M.K. Jones, A. Lung,
D. Mack (Co-spokesman), D. Meekins, J. Mitchell, W. Vulcan, S. Wood, C. Yan
Physics Division, TJNAF

H. Blok (Co-spokesman), B. Zihlmann
Faculteit Natuur- en Sterrenkunde, Vrije Universiteit
Amsterdam, The Netherlands

J. Arrington, D. Gaskell, H. Jackson, D. Potterveld
Argonne National Laboratory, Argonne, IL

P. Markowitz*, J. Reinhold*
Florida International University, Miami, FL

K. Assamagan, S. Avery, O.K. Baker*, M.E. Christy, W. Hinton, C. Keppel*, L.G. Tang*
Physics Department, Hampton University, Hampton, Virginia

W. Kim
Kyungbook University, Taegu, Korea

H. Breuer, C.C. Chang, N. Chant
University of Maryland, College Park, MD

J. Dunne*
Mississippi State University, Mississippi State, MS

A. Klein, K. Vansyoc
Old Dominion University, Norfolk, Virginia

R. Gilman*
Rutgers University, Piscataway, NJ

R. Asaturyan, H. Mkrtchyan, S. Stepanyan, V. Tadevosyan
Yerevan Physics Institute, Yerevan, Armenia

K. Gustafsson[1], G. Niculescu[2], I. Niculescu[3], J. Volmer[4]
[1] *W.K. Kellogg Radiation Laboratory, Caltech, Pasadena, CA*
[2] *Ohio University, Athens, OH*
[3] *George Washington University, Washington, DC*
[4] *DESY, Hamburg, Germany*

* *and Physics Division, TJNAF*

Summary

At JLab, we have a unique opportunity to dramatically improve the F_π database. Much can be learned about the usefulness of QCD sum rules and relativistic potential models for understanding the structure of the pion in the (presumably) difficult and non-perturbative Q^2 regime of 1-5 (GeV/c)^2.

This proposal deals with the continuation of our successful F_π program. Using the Hall C spectrometers and beam with energy up to 4.045 GeV, we have recently obtained a result (E93-021) for the charged pion form factor (F_π) up to Q^2=1.6 (GeV/c)^2 at W=1.95 GeV. Based on this result, a number of issues arise which we address in this proposal:

1. The E93-021 result extends the region of high quality F_π data from Q^2= 0.7 (GeV/c)^2 to 1.6 (GeV/c)^2. Even at Q^2= 1.6 (GeV/c)^2, the old Cornell F_π values are widely scattered, and are not based on a true L/T separation. (A certain recipe was taken for the transverse cross section, which according to the E93-021 results gives too small $\sigma_{\rm T}$ values.) The higher energy beam that is now available allows us to perform high quality F_π measurements with the existing Hall C instrumentation up to Q^2= 2.5 (GeV/c)^2. This is the region where the theoretical calculations for F_π begin to diverge, and data are used as input to several of the QCD-related models of F_π to constrain the treatment of the soft contributions.

2. The higher-energy beam also allows us to perform high quality measurements at higher W than in E93-021. As extraction of F_π from the data inherently depends upon a model of the $p(e,e'\pi^+)n$ reaction, the higher W is advantageous because it allows measurements to be taken closer to the π^+ pole than otherwise, where t-channel contributions dominate.

   In addition, for the E93-021 result, the Regge model used in the extraction of the form factor had a shallower $d\sigma_L/dt$ dependence than the data, resulting in a F_π model dependence comparable to the experimental uncertainty. A likely reason for this is that the value $W = 1.95$ GeV of the measurement was a bit low, and resulted in resonance contributions to the cross section. This model dependence is expected to be reduced if the measurements are performed at higher W, as proposed here.

In 1996, we received approval for a 13 day beam extension to the E93-021 run to obtain data at the highest Q^2 then accessible with 5 GeV beam. However, beam scheduling constraints and the ongoing analysis of the E93-021 data precluded our use of this beam before the jeopardy rule time limit. We are now requesting time to extend the F_π measurements using up to 5.3 GeV beam, as well as improved priority, so that the experiment can be performed in a timely manner. The measurements we propose break down as follows:

Q^2 (GeV/c)^2	W (GeV)	$-t$ (GeV/c)^2	ϵ	Total Hours
2.5	2.22	0.189	0.540	132
			0.277	140
2.0	2.22	0.133	0.571	60
			0.292	104
1.6	2.22	0.093	0.600	31
			0.316	38
Total				21 days

1 Introduction

1.1 Scientific motivation

The π^+ electric form factor is a topic of fundamental importance to our understanding of hadronic structure. It is well known [1] that the asymptotic behavior is rigorously calculable in perturbative QCD (pQCD), with value

$$F_\pi \rightarrow \frac{8\pi\alpha_s f_\pi^2}{Q^2},$$

where $f_\pi = 133$ MeV is the $\pi^+ \rightarrow \mu^+\nu$ decay constant. This result is in principle exact, and is dependent only on the assumption of quark asymptotic freedom.

The theoretical prediction for F_π at experimentally accessible Q^2 is less certain, as soft scattering contributions, such as gluonic effects, must be explicitly taken into account. After years of theoretical effort, there has been considerable progress in our understanding around which value of Q^2 the hard scattering (asymptotic QCD) part of the pion form factor will dominate. For example, Jakob and Kroll [2] found that a self consistent treatment of the pQCD contribution to the pion form factor in the few GeV region requires the inclusion of both Sudakov corrections and the transverse momenta of the quarks, leading to values of Q^2F_π of about 0.08 around Q^2=2 (GeV/c)^2, much smaller than the data, which give about 0.4. Recently those calculations were extended to next-to-leading order [3, 4]. The latter calculation, which uses also slightly different assumptions about the transverse momenta in the pion wave function, yields a value of Q^2F_π of about 0.19 around Q^2=2 (GeV/c)^2, still less than half of the experimental value.

The most interesting question then, as far as Jefferson Laboratory is able to address, is the description of $F_\pi(Q^2)$ in the gap between the "soft" and "hard" regions. This is a difficult and poorly understood region. Braun, Khodjamirian, and Maul [5] performed light-cone sum rule calculations up to twist 6, and found that the hard contributions of higher twist strongly cancel the soft components, even at relatively modest Q^2. Their LCSR prediction gives Q^2F_π of about 0.3 around Q^2=2 (GeV/c)^2, while the non-perturbative correction to it yields another 0.1. Calculations within QCD sum rules [6] give similar results.

On the 'soft' front, constituent quark model (CQM) calculations within the light-front formalism with a one-gluon-exchange term and a linear confining potential [7] had to include a quark form factor (with a rms radius of 0.48 fm) in order to be able to reproduce the pion radius (0.66 fm) and to avoid much too high values of F_π at large Q^2. The Bethe-Salpeter Equation (BSE) calculations by [8], which employ a separable interaction and include a dynamical quark mass, used two adjustable parameters (m_q and the cut-off parameter Λ in the separable interaction) to reproduce the pion radius and the then existing data at higher Q^2. Recently, Maris and Tandy [9] used the Bethe-Salpeter plus Schwinger-Dyson equations with a momentum dependent dressing of the quarks to determine the pion form factor. The model's parameters are adjusted to reproduce m_π, f_π, and $< \bar{q}q >$, then the predicted pion radius and F_π at higher Q^2 are in very good agreement with the E93-021 data.

Extending the range with reliable experimental data to values of Q^2 beyond where they exist now is clearly needed to delineate the role of hard versus soft contributions at intermediate Q^2, and so aid the further development and tests of these models.

The situation for the nucleonic form factors is even more complicated. Firstly, their asymptotic behavior is not predicted in such an unequivocal manner. Secondly, the greater number of valence quarks in the nucleon means that the asymptotic regime will be reached at much higher values of Q^2, at least 100 (GeV/c)^2[10]. Because of these reasons, we think that the pion is the first choice when one wants to investigate the transition from a 'soft' to a pQCD description of a hadronic form factor.

1.2 Description of the E93-021 F_π Result

At very low values of Q^2, F_π is determined by the charge radius of the pion. Up to Q^2= 0.28 (GeV/c)^2, F_π was measured directly from the scattering of high-energy pions from atomic electrons [11]. For the determination of the pion form factor at higher values of Q^2, one has to use high-energy electroproduction of pions on a nucleon, i.e. employ the ^{1}H$(e,e'\pi^+)n$ reaction. For selected kinematical conditions, this process can be described as quasi-elastic scattering of the electron from a virtual pion in the proton. In the t-pole approximation, the longitudinal cross section $\sigma_{\rm L}$ is proportional to the square of the pion form factor. Thus, the pion form factor has been studied for Q^2 values from 0.4 to 9.8 (GeV/c)^2 at CEA/Cornell [12], and for Q^2= 0.35 and 0.7 (GeV/c)^2 at DESY [13, 14]. In the DESY experiment, a longitudinal/transverse (L/T) separation was performed by taking data at two values of the electron energy for each Q^2. In the experiments done at CEA/Cornell, this was done in a few cases only, and even then the resulting uncertainties in $\sigma_{\rm L}$ were so large that the L/T separated data were not used. Instead, for the actual determination of the pion form factor $\sigma_{\rm L}$ was calculated by subtracting from the measured (differential) cross section a $\sigma_{\rm T}$ that was assumed to be proportional to the total virtual photon cross section. No uncertainty in $\sigma_{\rm T}$ was included in this subtraction. This means that the historical values of F_π above Q^2= 0.7 (GeV/c)^2 are not based on L/T separated cross sections. This, together with the already relatively large statistical (and systematic) uncertainties of those data, precludes a meaningful comparison with theoretical calculations in that region.

The high quality CEBAF electron beam and Hall C magnetic spectrometers allowed us to determine L/T separated cross sections with high accuracy and thus to study the pion form factor in the important regime of Q^2= 0.6 - 1.6 (GeV/c)^2, at a central value of the invariant mass W of 1.95 GeV [15]. The full details are given in [16]; what follows is a brief synopsis of our result.

The cross section for pion electroproduction can be written as

$$\frac{d^3\sigma}{dE'd\Omega_{e'}d\Omega_\pi} = \Gamma_V \frac{d^2\sigma}{dtd\phi}, \tag{1}$$

where Γ_V is the virtual photon flux factor, ϕ is the azimuthal angle of the outgoing pion with respect to the electron scattering plane and t is the Mandelstam variable $t = (p_\pi - q)^2$. The two-fold differential cross section can be written as

$$\begin{aligned} 2\pi\frac{d^2\sigma}{dtd\phi} &= \epsilon\,\frac{d\sigma_{\rm L}}{dt} + \frac{d\sigma_{\rm T}}{dt} + \sqrt{2\epsilon(\epsilon+1)}\,\frac{d\sigma_{\rm LT}}{dt}\cos\phi \\ &\quad +\epsilon\,\frac{d\sigma_{\rm TT}}{dt}\,\cos 2\phi. \end{aligned} \tag{2}$$

The cross sections $\sigma_X \equiv \frac{d\sigma_X}{dt}$ depend on W, Q^2 and t. The longitudinal cross section $\sigma_{\rm L}$ is dominated by the t-pole term, which contains F_π. The ϕ acceptance of the experiment allowed the combination $\epsilon\sigma_{\rm L}+\sigma_{\rm T}$, and the interference terms $\sigma_{\rm LT}$ and $\sigma_{\rm TT}$ to be determined. Since data were taken at two energies at every Q^2, $\sigma_{\rm L}$ could be separated from $\sigma_{\rm T}$ by means of a Rosenbluth separation.

Sieve-slit calibrations and measurements of the overdetermined ^{1}H$(e,e'p)$ reaction were critical in several applications. The beam momentum and the spectrometer central momenta were determined absolutely to 0.1%, while the incident beam angle and spectrometer central angles were absolutely determined to better than 1 mrad. The spectrometer acceptances were checked by comparison of data to MC simulations. Finally, the overall absolute cross section normalization was checked. The calculated yields for $e+p$ elastics agreed to better than 2% with the ones predicted employing a parameterization of the world data [17].

A representative example of the cross section as function of ϕ is given in Figure 1. The dependence on ϕ was used to determine the combination $\sigma_{\rm uns} = \sigma_{\rm T} + \epsilon\sigma_{\rm L}$ and the interference terms $\sigma_{\rm LT}$ and $\sigma_{\rm TT}$ at both the high and low electron energy for five t bins at each Q^2 point. The statistical uncertainty in the $\sigma_{\rm uns}$

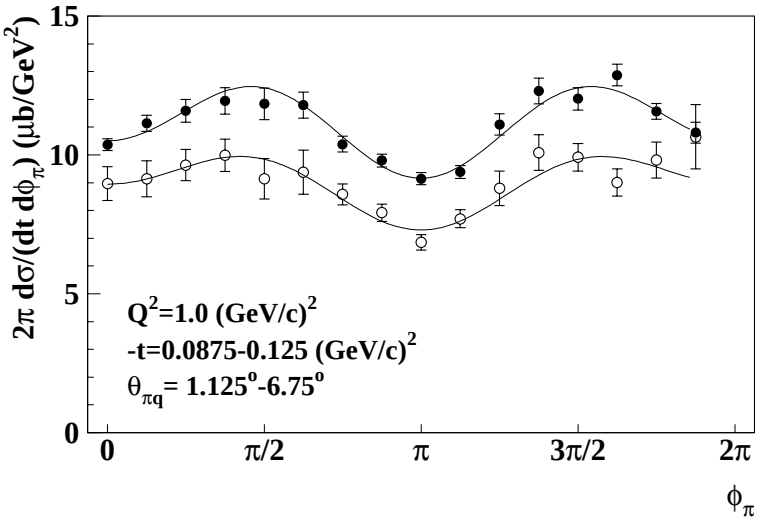

Figure 1: ϕ dependence of $\frac{d^2\sigma}{dtd\phi}$ at Q^2=1.0 (GeV/c)^2 for high and low ϵ (filled and empty circles, resp.). The curves represent the fit result.

cross sections ranges from 2 to 5%. Furthermore, there is a total systematic uncertainty of about 3%, the most important contributions being: simulation of the detection volume (2%), dependence of the extracted cross sections on the MC cross section model (typically less than 2%), target density reduction (1%), pion absorption (1%), pion decay (1%), and the simulation of radiative processes (1%) [16]. Since the same acceptances in W and Q^2 and the same average values $\bar{W}$ and $\bar{Q}^2$ were used at both energies, $\sigma_{\rm L}$ and $\sigma_{\rm T}$ could be extracted via a Rosenbluth separation.

These cross sections are displayed in Figure 2. The error bars represent the combined statistical and systematic uncertainties. Since the uncertainties that are uncorrelated in the measurements at high and low electron energies are enlarged by the factor $1/(\Delta\epsilon)$ in the Rosenbluth separation, where $\Delta\epsilon$ is the difference (typically 0.3) in the photon polarization between the two measurements, the total error bars on $\sigma_{\rm L}$ are typically about 10%.

The experimental data were compared to the results of a Regge model by Vanderhaeghen, Guidal and Laget (VGL) [18]. In this model, the pion electroproduction process is described as the exchange of Regge trajectories for π and ρ like particles. The only free parameters are the pion form factor and the $\pi\rho\gamma$ transition form factor. The model globally agrees with existing pion photo- and electroproduction data at values of W above 2 GeV. The VGL model is compared to the data in Figure 2. The value of F_π was adjusted at every Q^2 to reproduce the $\sigma_{\rm L}$ data at the lowest value of t. The transverse cross section $\sigma_{\rm T}$ is underestimated, which can possibly be attributed to resonance contributions at $W = 1.95$ GeV that are not included in the Regge model. Varying the $\pi\rho\gamma$ transition form factor within reasonable bounds changes $\sigma_{\rm T}$ by up to 30%, but has a negligible influence on $\sigma_{\rm L}$, which is completely determined by the π trajectory. The t-pole dominance of the data was checked by studying the reactions ^{2}H$(e,e'\pi^+)nn$ and ^{2}H$(e,e'\pi^-)pp$, which gave within the uncertainties a ratio of unity for the longitudinal cross sections (this will be discussed in more detail at a point later in the proposal). Hence the VGL model is still considered to be a good starting point for determining F_π.

The comparison with the $\sigma_{\rm L}$ data shows that the t dependence in the VGL model is less steep than that of the experimental data. The question is then how to determine a trustworthy value of F_π. As suggested by the analysis [19] of older data, where a similar behavior was observed, we attributed the discrepancy

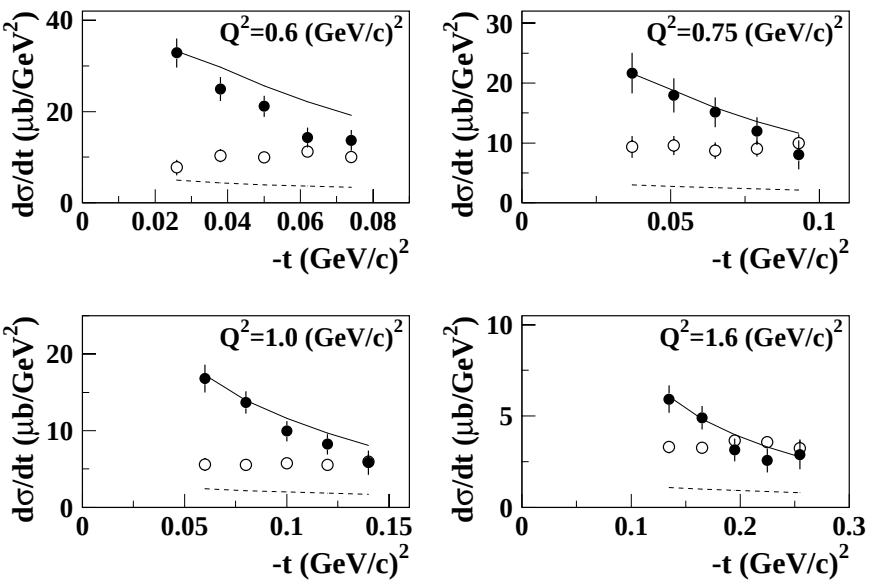

Figure 2: Separated cross sections $\sigma_{\rm L}$ and $\sigma_{\rm T}$ (full and open symbols, resp.) compared to the Regge model (full curve for L, dashed curve for T).

between the data and VGL to the presence of a negative background contribution to the longitudinal cross section, presumably again due to resonances. With this assumption we proceeded on two paths. First, we fitted the VGL prediction for $\sigma_{\rm L}$ to the data by adjusting F_π at the lowest $|t|$ bin, as shown in Fig. 2, where it is assumed to be most reliable, owing to the dominant t pole behavior. However, since there is no reason to believe that the (negative) background is zero at the lowest $-t$, the result is an underestimate for F_π. Secondly, F_π was determined adding a (Q^2 dependent) negative background to $\sigma_{\rm L}$(VGL) and fitting it together with the value of F_π. The background term was taken to be independent of t. This was suggested by looking at the 'missing background' in $\sigma_{\rm T}$, i.e., the difference between the data and VGL for $\sigma_{\rm T}$. That background is almost constant or slightly rising with $|t|$. Then, assuming that the background in $\sigma_{\rm L}$ has a similar t dependence, a constant background leads to an overestimate of F_π. Our best estimate for F_π is taken as the average of the two results. The model uncertainty (in relative units) is taken to be the same for the four Q^2 points, and equal to one half of the average of the (relative) differences. The results are shown in the form of Q^2F_π in Fig. 3. The error bars were propagated from the uncertainties (statistical and systematic) on the cross section data. The model uncertainty is displayed as the gray bar. The fact that the value of F_π at Q^2= 0.6 (GeV/c)^2 is close to the extrapolation of the model independent data from [11], and that the value of the background term is lower at higher W (see below), gives some confidence in the procedure used to determine F_π.

For consistency, we have re-analyzed the older L/T separated data at Q^2= 0.7 (GeV/c)^2 taken at W = 2.19 GeV from DESY [14]. We took their published cross sections and treated them in the same way as ours. The background term in $\sigma_{\rm L}$ was found to be smaller than in the Jefferson Lab data, presumably because of the larger value of W of the DESY data, and hence the model uncertainty is smaller, too. The resulting best value for F_π, also shown in Fig. 3, is larger by 12% than the original result, which was obtained by using the Born term model by Gutbrod and Kramer [19]. Here it should be mentioned that those authors used a phenomenological t-dependent function, whereas the Regge model by itself gives a good description of the t dependence of the (unseparated) data from Ref. [12].

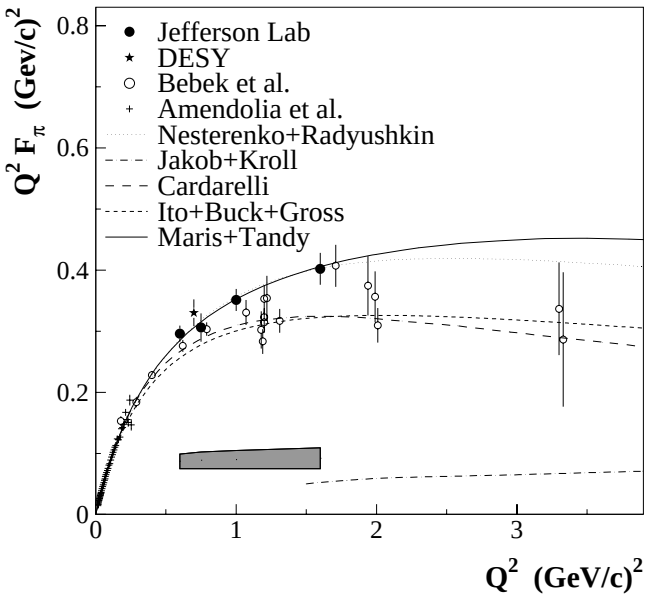

Figure 3: The Jefferson Laboratory and re-analyzed DESY values for F_π as well as (model-independent) data from Ref. [11] [+]. The old Cornell data are shown for comparison only. The high quality results are compared to some representative theoretical calculations. The E93-021 model uncertainty is indicated at the bottom of the figure. A monopole behavior of the form factor obeying the measured charge radius is almost identical to the Maris and Tandy curve.

The data for F_π in the region of Q^2 up to 1.6 (GeV/c)^2 globally follow a monopole form obeying the pion charge radius of 0.662 fm [11]. It should be mentioned that the older Bebek data in this region suggested lower F_π values. However, as mentioned, they did not use L/T separated cross sections, but took a prescription for $\sigma_{\rm T}$. Our measured data for $\sigma_{\rm T}$ indicate that the values used were too high, so that the values for F_π came out systematically low.

In Fig. 3 these results are also compared to a number of theoretical calculations. Both the Maris and Tandy (M&T) and the Nesterenko and Radyushkin (N&R) models provide good descriptions of the data. M&T is based on the Bethe-Salpeter equation with dressed quark and gluon propagators, and includes parameters that were determined without the use of F_π data. N&R uses a QCD sum rule calculation for the soft contribution to F_π as well as an asymptotically dominant hard gluon exchange term. High quality data are clearly needed to pin down with greater precision the form factors in the multi (GeV/c)^2 range.

2 The Proposed Experiment

Given the present situation, two issues arise:

1. Data for F_π at higher values of Q^2 are needed to discriminate between the various models for F_π, and so learn about the treatment of the soft contributions. As mentioned, the old Cornell F_π values show a lot of scatter, are not based on a true L/T separation, and their assumed transverse cross section is likely incorrect, resulting in an erroneous F_π extraction. The higher beam energy that is now available will allow measurements with the existing Hall C instrumentation up to Q^2= 2.5 (GeV/c)^2.

2. As mentioned when explaining our determination of F_π from the measured $\sigma_{\rm L}$, E93-021 likely suffered from the relatively low value of W used. A higher W will take us farther from the resonance region, and at the same time allow measurements to be obtained closer to the π^+ pole. Both points are expected to reduce the model uncertainty when using the model to extract F_π. L/T separations at $W = 2.22$ GeV are now feasible. Combining the Q^2= 1.6 (GeV/c)^2 measurements at $W = 1.95$ GeV (from E93-021) with those at $W = 2.22$ GeV (proposed here) will provide valuable information on the W dependence of the reaction, and so aid the extraction of the form factor. The data at higher Q^2 will be also be taken at $W = 2.22$ GeV.

2.1 Kinematics

In this experiment, we will make coincidence measurements between charged pions in the HMS and electrons in the SOS. Since the HMS will detect pions along the direction of $\vec{q}$, the dominant contribution will be due to the pion pole diagram. Only events with θ_{pq} near zero degrees are useful, so a high luminosity spectrometer system like the HMS-SOS is well suited to the measurement. Because σ_L must be separated, two beam energies are needed for each Q^2. Table 1 shows the 'near parallel' kinematics settings proposed for the experiment.

In comparison with E93-021, we propose to take the new measurements at higher W, 2.22 GeV. This higher W will work to our advantage in two ways. (1) The higher W will allow data to be obtained at smaller $|t|$, closer to the pion pole. A comparison of the existing and proposed Q^2= 1.6 (GeV/c)^2 settings shows that W=1.95 allows $-t = 0.150$, while W=2.22 allows $-t = 0.093$ (GeV/c)^2. Thus, the π^+ pole term will dominate $\sigma_{\rm L}$ even strongly than it did in E93-021, resulting in a more reliable F_π extraction. (2) Also, at higher W the resonant contributions to the data should be smaller, and we anticipate that this will improve the agreement between the $\sigma_{\rm L}$ data and the Regge model, which does not include resonant contributions. We note that in our re-analysis of the DESY $W = 2.19$ GeV data [14], the agreement between the Regge model and the $\sigma_{\rm L}$ data was better than for the E93-021 data, resulting in a 35% smaller model dependence in the extracted F_π value. Finally, the two measurements at Q^2= 1.6 (GeV/c)^2 will allow the W dependence of the reaction to be obtained, which will further test the validity of the reaction model used.

The proposed kinematics were arrived at by taking into account the following constraints:

- the SOS spectrometer is limited by saturation to a field lower than 1.80 GeV/c. By maintaining a maximum momentum setting no higher than 1.76 GeV/c, we expect the correction to the SOS central momentum due to the decrease of the effective field length to be no larger than 1.1%.

- the HMS will detect pions at small forward angle (i.e. low $-t$). We are constrained by the minimum HMS forward angle of 10.5^o (for small angle mode).

Given these constraints, W=2.22 GeV and Q^2=2.5 (GeV/c)^2 are essentially the maximum values that allow us to span a reasonable range of ϵ.

Table 1: 'Near parallel' kinematics settings for $N(e,e'\pi^{\pm})N$. Additional runs at other kinematics are also required, as described in the text. No optimization of beam energies has been performed to minimize accelerator tuning overhead. We recognize that this will have to be done at the time the experiment is scheduled, in concert with the requirements of the experiments running in parallel in Halls A and B. Through the judicious choice of W, Q^2 and ϵ close to these values, we are able to perform the experiment with just three linac gradient values.

Q^2	W	$\|t\|$	E_e	$\theta_{e'}$	$E_{e'}$	θ_π	θ_{HMS}	p_π	ϵ
(GeV/c)^2	(GeV)	(GeV/c)^2	(GeV)	(deg)	(GeV)	(deg)	(deg)	(GeV/c)	
This proposal									
2.50	2.22	.189	5.25	30.14	1.76	13.34	14.56	3.385	.540
2.50	2.22	.189	4.29	50.50	0.80	9.28	10.50	3.385	.277
2.00	2.22	.133	4.98	27.66	1.76	13.40	14.63	3.148	.571
2.00	2.22	.133	3.99	47.68	0.77	9.27	10.50	3.148	.292
1.60	2.22	.093	4.77	25.22	1.76	13.28	14.49	2.956	.600
1.60	2.22	.093	3.77	43.88	0.76	9.29	10.50	2.956	.316
Completed E93-021 - for comparison									
1.60	1.95	.150	4.045	28.48	1.634	16.63	16.63	2.326	.6263
1.60	1.95	.150	3.005	56.49	0.594	10.49	10.50	2.326	.2722
1.00	1.95	.071	3.548	25.41	1.457	15.65	15.65	2.048	.6469
1.00	1.95	.071	2.673	47.26	0.582	10.63	10.63	2.048	.3272
0.75	1.95	.044	3.548	21.01	1.590	15.45	15.45	1.929	.7042
0.75	1.95	.044	2.673	36.50	0.715	11.46	11.46	1.929	.4295
0.60	1.95	.030	3.548	18.31	1.670	14.97	14.97	1.856	.7369
0.60	1.95	.030	2.445	38.40	0.567	9.99	10.50	1.856	.3749

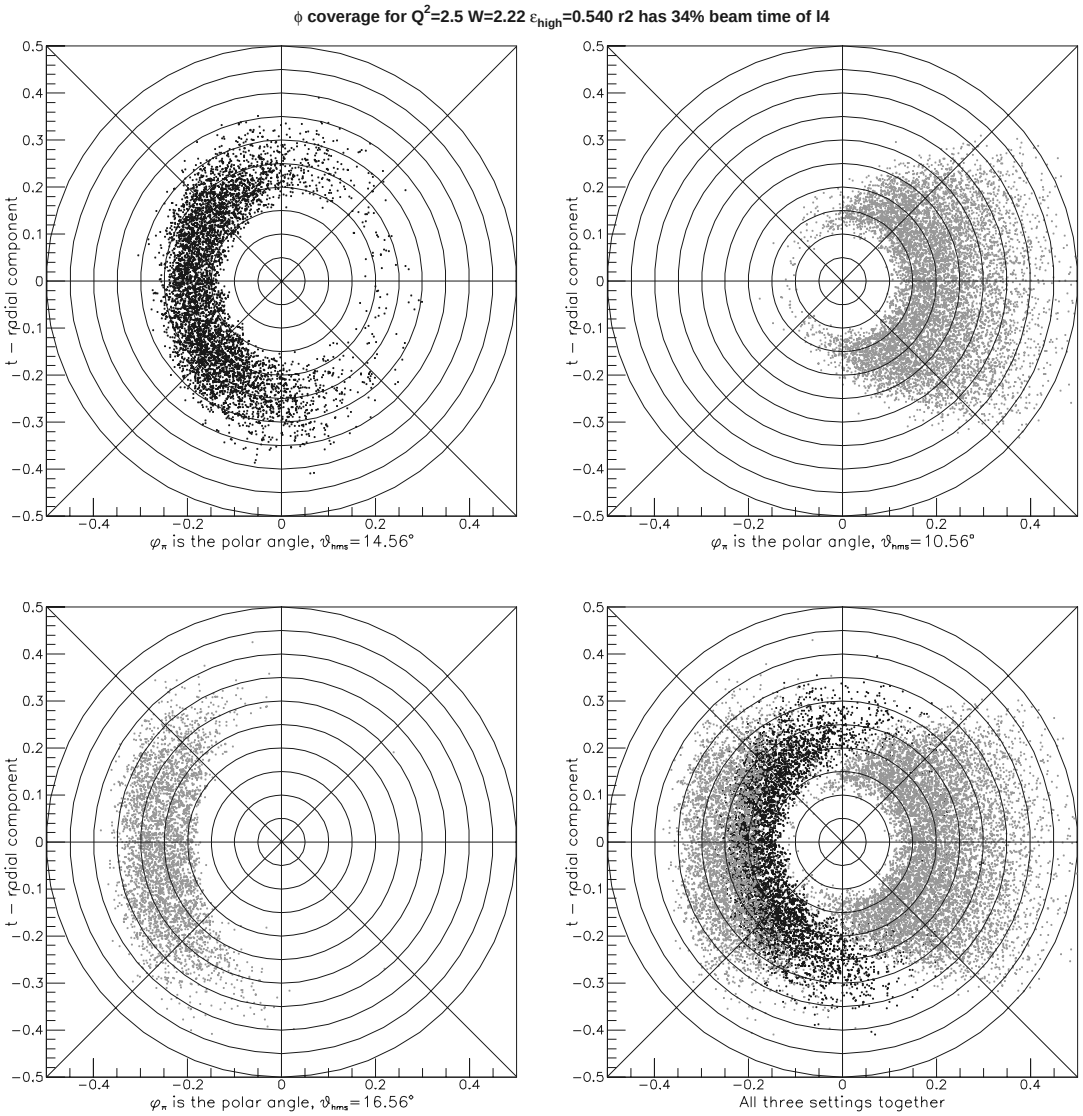

Figure 4: ϕ versus $-t$ coverage at Q^2= 2.5 (GeV/c)^2 and high ϵ. The figures are polar plots, with $-t$ as the radius, and ϕ as the angle. Cuts were placed to match W-Q^2 range of the low ϵ setting. Each radial division corresponds to $-t = .05$. The four panels are as follows: *Upper left:* ϕ range in the 'near parallel' kinematic setting ($\theta_{HMS} = 14.56^o$, $\theta_{\pi q} = 1.2^o$). As expected, the data are centered about $\phi = 180^o$. *Upper right:* Data near $\phi = 0$ are obtained by moving the HMS to 10.56^o ($\theta_{\pi q} = -3^o$). *Lower left:* Additional data are taken at $\theta_{HMS} = 16.56^o$ ($\theta_{\pi q} = +3^o$). *Lower right:* The superposition of the three HMS settings shows good ϕ coverage for the range $0.14 < |t| < 0.40$.

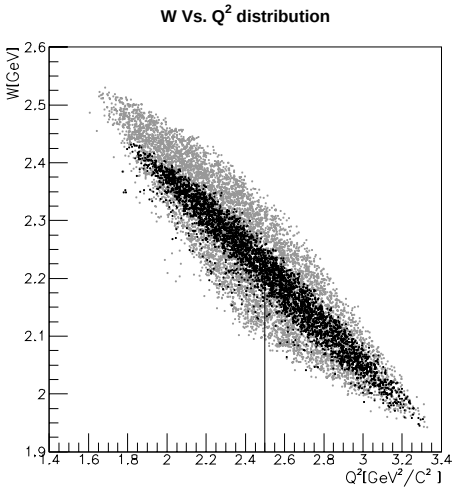

Figure 5: Q^2 versus W coverage for the 'near parallel' setting at Q^2= 2.5 (GeV/c)^2. The black points are the low ϵ setting, and the gray points are the high ϵ setting.

To extract F_π from the $\sigma_{\rm L}$ data, it is necessary to measure the $-t$ dependence of the reaction. Unfortunately, it is not possible to hold W and Q^2 fixed in parallel kinematics, and still vary $-t$. Therefore, it is necessary to obtain data for $\theta_{\pi q} \neq 0$, where σ_{LT} and σ_{TT} also contribute. Figure 4 shows simulated HMS+SOS data where θ_{HMS} is varied from the 'near parallel' kinematic position. Therefore, at each high ϵ setting in table 1 we will take additional data at $\theta_{\pi q} = \pm 3^o$. At low ϵ, the HMS forward angle constraint will only allow data at $\theta_{\pi q} = +3^o$ to be taken. The excellent ϕ coverage allows σ_{LT} and σ_{TT} to be obtained in an efficient manner versus $-t$.

The two measurements at high and low ϵ allow $\sigma_{\rm L}$ and $\sigma_{\rm T}$ to be extracted from the data. Figure 5 shows the range of Q^2 and W accepted by the experiment at Q^2= 2.5 (GeV/c)^2. Cuts are first placed on the data to equalize the range measured by the two settings. Figure 6 shows the final $-t$ range over which a full L, T, LT, and TT separation can be performed for the three proposed Q^2 settings. This should be compared with $-t$ range of the E93-021 data for the $Q^2 = 1.6$ case in figure 2.

As mentioned earlier, it is imperative to test the t-channel dominance of the $\sigma_{\rm L}$ data by measuring the ratio

$$R_l = \frac{\sigma_L(\gamma_v + n \rightarrow \pi^- + p)}{\sigma_L(\gamma_v + p \rightarrow \pi^+ + n)} = \frac{|A_v - A_s|^2}{|A_v + A_s|^2}.$$

with a deuterium target. The t-channel diagram is a purely isovector process, and so at small $|t|$, R_l should be near unity. Isoscalar backgrounds are expected to be suppressed by the L response function extraction. Nonetheless, if they are present to any significant degree, they will result in a dilution of the ratio. These tests were also performed in E93-021, and preliminary $\sigma_{\rm L}$ ratios are shown in figure 7. The measured ratio is consistent with unity, as well as with Regge model predictions, over the entire measured range of $|t|$. Repeating this test at Q^2= 2.0 and 2.5 (GeV/c)^2 will lend confidence in the F_π value extracted from the experiment. In order to improve the statistical precision of this test, we propose to obtain more events than were obtained in E93-021.

Finally, with the assistance of the Regge (or other available) model, F_π can then be extracted from the

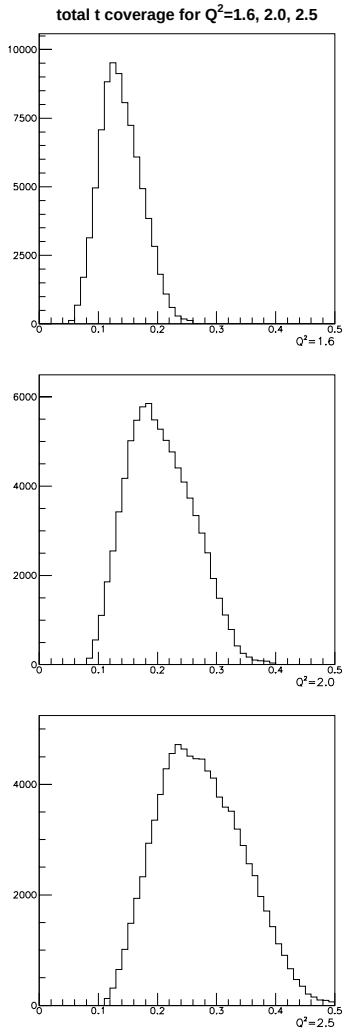

Figure 6: Total $-t$ coverage at Q^2= 1.6, 2.0 and 2.5 (GeV/c)^2 after combining the HMS+SOS 'near parallel' and $\theta_{\pi q} = \pm 3^o$ data, and after application of all analysis cuts to equalize the spectrometer acceptance at high and low ϵ.

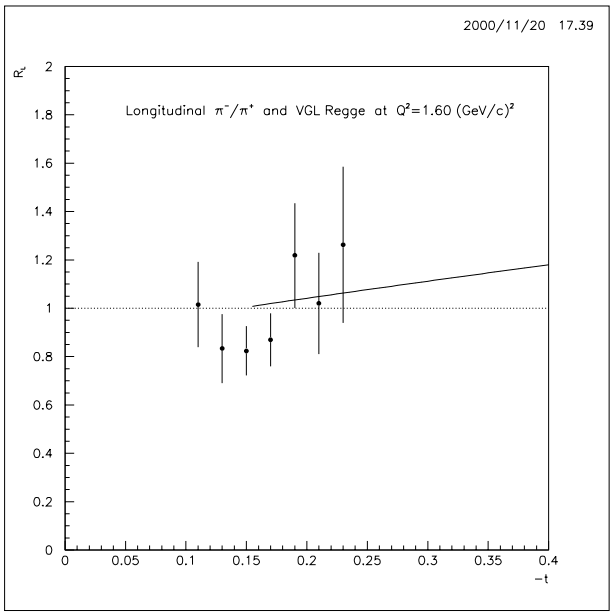

Figure 7: $-t$ dependence of the longitudinal π^-/π^+ ratio at Q^2 1.6 (GeV/c)^2, as measured in E93-021. The data shown are preliminary. The curve is a prediction of the Regge model. The consistency of the measured experimental ratio with unity indicates that the longitudinal data are dominated by the t-channel diagram.

Table 2: Performance of the HMS (pt-to-pt, small angle mode) and SOS (pt-to-pt). Resolutions are all σ. The solid angle is defined by octagonal apertures of densimet in both arms.

	$\Delta p/p$	$dx'tgt$	$dy'tgt$	$dYtgt$	Δp	$\Delta\Theta$	$\Delta\Phi$	$\Delta\Omega$
		(mrad)	(mrad)	(cm)	(GeV/c)	(mrad)	(mrad)	(msr)
HMS	$0.6{\cdot}10^{-3}$	1.5	0.7	0.15	$\pm$10%	$\pm$69.5	$\pm$27.2	6.62
SOS	$0.7{\cdot}10^{-3}$	0.2	2.0	0.20	$\pm$ 15%	$\pm$37.5	$\pm$57.5	7.55

$-t$ dependence of the $\sigma_{\rm L}$ data.

2.2 Instrumentation

Spectrometers

Table 2 contains the actual performance of the spectrometers for momenta typical of this experiment.

As in E93-021, the HMS will be operated in small angle mode ($\theta_{min} = 10.5$ degrees) with the quad string pulled back 40 cm. The spectrometer has remained in this configuration since E93-021, and so needs no reconfiguration. Extensive sieve slit data were taken in E93-021, and accurate HMS matrix elements were determined between 1.85 and 2.33 GeV/c [16]. This experiment requires a maximum HMS momentum of 3.39 GeV/c. In recent experiments no saturation effects have been seen in HMS up to even larger momenta, so we only plan to check the matrix elements by taking a set of sieve slit data at this (scattered electron) momentum. No need for full matrix element fitting is expected.

However, this experiment requires a maximum SOS momentum (1.76 GeV/c) considerably higher (in

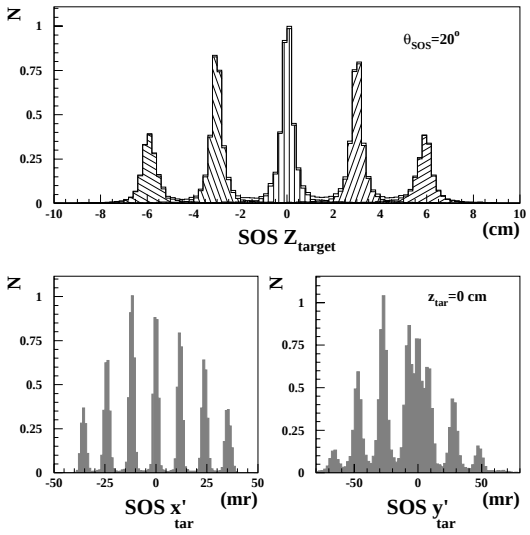

Figure 8: SOS quintar and sieve slit reconstruction from an E93-021 calibration run. Top: reconstruction of the quintar z_{tar} coordinate. The distribution shown is the sum of the five individual targets (hashed). Bottom: reconstruction of the vertical (left) and horizontal (right) sieve slit hole pattern.

saturation effects) than where matrix elements have been previously determined (1.65 GeV/c for angles and 1.4 GeV/c for δ). Based on our E93-021 experience, at this value we expect the correction to the SOS central momentum due to the decrease of the effective field length to be as large as 1.1%, which influences all matrix elements. For this reason, a full set of optical calibration measurements has to be done for the SOS at 1.76 GeV/c. These include: sieve-slit data for different positions of the vertex along the beam for the determination of the (y dependence of the) θ, ϕ matrix elements, and use of the elastic $^1H(e,e')$ peak at different scattering angles for the δ-matrix elements.

As in E93-021, we will use a special thin target assembly ("Quintar") to determine the spectrometer matrix elements. It defines five interaction points (values of y) along the beam axis (as well as serving as a dummy aluminum target imitating the walls of the LH_2 and LD_2 cells). Representative quintar and sieve slit reconstruction from E93-021 are shown in Fig. 8.

In addition, hydrogen elastics data will be taken both with and without the sieve slit. The elastics coincidence data are over-constrained, and so are a critical check on the determination of the beam momentum and spectrometer central momenta and angles. Furthermore the elastic cross section is known, so that it can be used to check if the spectrometer acceptances are well understood. These data are of vital importance to achieve the low level of systematic error anticipated for this experiment.

Target

A liquid hydrogen target will be used to make cross-section measurements of $\gamma_v + p \to \pi^+ + n$. We will use a liquid deuterium target to determine the separated ratios

$$R_i = \frac{\sigma_i(\gamma_v + n \to \pi^- + p)}{\sigma_i(\gamma_v + p \to \pi^+ + n)} \qquad i = L, T.$$

The Hall C cryogenic target will be used with 4 cm cells. The target windows will be viewed by both spectrometers at all angle settings, so target empty measurements must also be made. We expect the

Table 3: Hall C detection efficiencies.

HMS tracking	0.95
SOS tracking	0.95
pion absorption	0.95
pion decay (typical)	0.85
HMS acceptance for δ=-10% to +10%	0.9
SOS acceptance for δ=-15% to +15%	0.9

resulting luminosity and rate to be well within the operational experience of E93-021, and other Hall C experiments.

Beam

The standard Hall C beamline hardware will be used. In addition to the raster systems, super-harps permit accurate measurements of beam size and angle. Passive RF cavities absolutely normalized with an Unser monitor and an accurate current reference provide average current measurements with errors of 100-200 nA (i.e. less than 0.4% at 50 μA). The arc energy measurement system will be used to determine the absolute beam energy to 0.1%. Accelerator BPM information is also available in our data stream via EPICS, so we can monitor beam energy drifts (often as much as $5{\cdot}10^{-4}$ due to RF phase instabilities).

2.3 Rates

Our rate estimates are based on SIMC Monte Carlo simulations of the Hall C spectrometers, incorporating the actual spectrometer acceptances, and parameterized E93-021 cross sections [16]. We also assume:

- The target thickness is 4 cm.
- The beam current is 75 μA.

Spectrometer acceptances were already given in Table 2; kinematic settings are found in Table 1; detection efficiencies are found in Table 3; count rate estimates are summarized in Table 4.

Singles rates in the HMS and SOS were examined for $p(e,e'\pi^+)$ data taking [21], and are listed in table 5. The total singles rates are well below the capability of the detector packages, which were constructed with multi-MHz singles rates in mind. For the purpose of calculating online random coincidence rates, the HMS trigger rate was taken as equal to the raw trigger rate. (We do not distinguish pions and protons in the HMS online.) Assuming an online π^- rejection rate of 25:1, the SOS trigger rate was taken to be electrons plus $\pi^-/25$. The random coincidence rate is then given by (HMS trigger rate)(SOS trigger rate)Δt, where the coincidence resolving time Δt = 40 nsec. The resulting online real + random rates are well below the capability of our data acquisition system. Offline, the relevant resolving time is 2 nsec and the reals to randoms ratio for electron-pion coincidences after missing mass cuts will only be a few percent for $p(e,e'\pi^+)$. Random backgrounds will be an order of magnitude larger for $d(e,e'\pi^\pm)$ because of the larger missing mass cut necessary.

2.4 Particle Identification

The HMS will sit at very forward angles throughout the experiment. The detector package will be configured for π^+ or π^- detection, the two polarities presenting very different cases for particle identification. In the positive polarity case, the ratio π^+/p is of order 1 with a negligible positron fraction. When the HMS is

Table 4: Real $p(e,e'\pi^+)n$ coincidence rates in parallel kinematics after application of cuts to equalize the $\Delta Q^2 \Delta W$ acceptance at low and high ϵ. The E93-021 rates are those actually observed in the experiment, included for comparison. The rates for this proposal are from a SIMC simulation incorporating parameterized E93-021 cross sections, the actual spectrometer acceptances and the tracking and π absorption corrections from table 3. All rates assume 4 cm LH_2 target and 75 μA beam current.

Q^2 (GeV/c)^2	W (GeV)	ϵ	$d\sigma/dt$ ($\mu b/GeV^2$)	Rate (Hz) $\times\Delta Q^2\Delta W$	Hours per 30,000 evts
This proposal					
2.50	2.22	0.540	8.7	0.9	9.4
		0.277	4.5	0.4	21.9
2.00	2.22	0.571	7.8	1.4	6.1
		0.292	5.3	0.6	16.1
1.60	2.22	0.600	10.7	2.5	3.4
		0.316	7.2	0.9	9.8
Actual E93-021 Rates - for comparison					
1.60	1.95	0.626	5.6 ± 0.2	2.5	3.3
		0.272	4.5 ± 0.1	0.6	13.9
1.00	1.95	0.647	12.2 ± 0.3	4.6	1.8
		0.327	9.0 ± 0.3	1.6	5.2
0.75	1.95	0.704	19.6 ± 0.5	9.3	0.9
		0.430	15.4 ± 0.4	5.2	1.6
0.60	1.95	0.737	26.6 ± 0.7	18.5	0.6
		0.375	18.6 ± 0.5	4.0	2.1

Table 5: Projected singles and accidental coincidence rates assuming 75 μA beam on 4 cm hydrogen target and the detection efficiencies in table 3. The coincidence rate assumes a resolving time of 40 ns, and corresponds to the online rate only; offline cuts will reduce this number to a few percent of the reals, as indicated in figure 9.

ϵ	SOS e^- rates Hz	SOS π^- rates Hz	HMS π^+ rates Hz	HMS Proton rates Hz	Random coinc. $(e^- + \pi^-/25)\cdot(\pi^+ + \mathrm{p})$ Hz
$Q^2 = 2.5 GeV^2/c^2, W = 2.2 GeV$					
0.540	1000	13k	5.8k	5.6k	0.7
0.277	220	59k	11k	8.2k	2.0
$Q^2 = 2.0 GeV^2/c^2, W = 2.2 GeV$					
0.571	1800	20k	9.0k	8.0k	1.8
0.292	280	83k	14k	10k	3.5
$Q^2 = 1.6 GeV^2/c^2, W = 2.2 GeV$					
0.600	3000	33k	13k	11k	4.2
0.316	460	110k	18k	13k	6.0

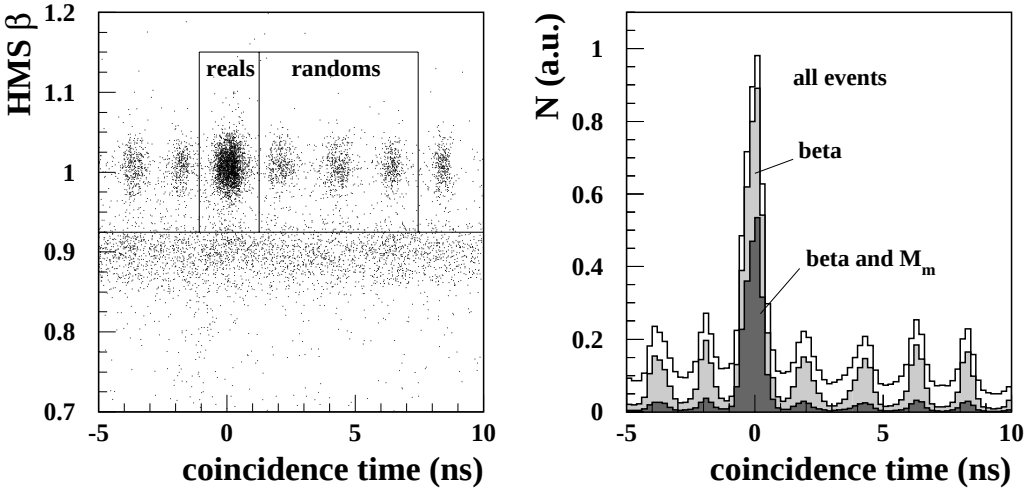

Figure 9: Actual E93-021 coincidence timing spectra. Left: HMS β versus coincidence time, clearly showing the real electron-pion coincidences. The continuous band below $\beta = 0.925$ are protons which are rejected in the analysis. Right: Coincidence timing spectrum with reals at 0 ns. Both the HMS β cut and the cut on reconstructed missing mass mainly reduce the contribution of random events. The random background to the real coincidences varied between 2 and 5%, depending on the kinematic conditions.

tuned for π^-, the ratio e/π is expected to be of order 1 as well. While the primary event of interest will be HMS•SOS, various prescaled HMS and SOS singles events will also be taken in order to monitor the detector and trigger efficiencies and luminosity.

The HMS detector package consists of two wire chambers followed by an $X - Y$ scintillator hodoscope, a gas Cerenkov detector, another $X - Y$ hodoscope, and finally a Pb-glass shower counter. Using C_4F_{10} at 0.5 atmosphere in the gas Cerenkov, only electrons will emit Cerenkov light. Offline, the gas Cerenkov and Pb glass shower counter will be used to reject electrons. The primary (non-prescaled) HMS trigger for $\pi^\pm$ will be simply $S1 \bullet S2$. Only 3 of 4 scintillator arrays require hits, so the efficiency is 100%, even with a dead phototube. (If the e^-/π^- ratio is higher than expected, the gas Cerenkov can be used as a hardware electron veto as in E93-021.)

The SOS detector package is similar in principle to the HMS detector package, the main difference being that the gas Cerenkov employs Freon at 1 atmosphere. Because the SOS angle will vary from forward to backward angles, the ratio π^-/e varies from 10 to several hundred. We plan to reject pions at the hardware level, identifying an electron by either a high preshower signal OR a high gas Cerenkov signal. In this case, the primary (non-prescaled) SOS trigger will be $S1 \bullet S2 \bullet Electron$. π^- rejection rates of 25:1 should be possible without risking significant inefficiency. We will also allow a prescaled sample of pions to pass to monitor the trigger efficiency. The same electron trigger was successfully used in E93-021 [16]. After offline calorimeter, gas Cerenkov, coincidence time and missing mass cuts, the π^- contamination will be negligible, even in the worst case scenario.

In E93-021, we used TOF in the detector hut to do hadron identification, sucessfully removing all or most of the protons. However, at the higher hadron momenta of this experiment, TOF in the hadron arm detector hut is no longer sufficient to reliably and efficiently distinguish pions and protons offline. Of course we can obtain clean separation ($\geq 16\sigma$!) of real $e-\pi$ and real $e-p$ coincidences by using HMS-SOS coincidence time.

(Figure 9 shows the actual coincidence timing resolution obtained under similar conditions in E93-021.) The experiment could thus be successfully run without HMS hadron identification, the only disadvantage being that this would roughly double our (few percent) random background. However, our preference would be to install an aerogel detector in the HMS to distinguish pions and protons. An index of refraction of 1.03 will provide large signals for pions but not for protons. The design of the new aerogel detector is in progress and draws on our experience with the successful SOS aerogel detector as well as recent construction in Hall A.

2.5 Non-physics backgrounds

Once a combination of online hardware and offline software has determined that there was a coincidence between an electron in the SOS and pion in the HMS, there remain several backgrounds of the incoherent 'non-physics' variety: random coincidences and events from the target endcaps.

The electronic coincidence resolving window will be roughly 40 nsec. Offline our excellent coincidence time resolution enables us to reduce the relevent resolving time to 2 nsec with negligible inefficiency. This is the first level of suppression of random coincidences. A cut on the missing mass variable reduces the final random coincidence contamination to the few percent level. The missing (or undetected residual) mass is reconstructed from the final electron and detected hadron 4-momenta:

$$M_{res}^2 = P_{res}^2 = (P_e - P_{e'} + P_{tgt} - P_h)^2$$

The missing mass cut does a lot more than reduce random coincidences. To the extent that particle identification is flawless, real coincidences with larger inelasticity than $p(e,e'\pi^+)n$ (e.g. two pion electroproduction) are completely removed. (See Figure 10) The small contamination from the reaction $p(e,\pi^-\pi^+)p$, where the π^- is misidentified as an e^-, is heavily suppressed. Finally, model dependences of the experimentally determined cross sections due to radiative effects and decay muons are reduced as well.

We have chosen the target length to be 4 cm. This means that both spectrometers will view the end windows in all configurations, so window background subtractions are necessary. Because the aluminum windows are each 4 mils thick, the ratio of protons in the windows to protons in the liquid hydrogen is about 10%. However, in E93-021 the surviving window background for $p(e,e'\pi^+)n$ after cuts was found to be only 1% [16]. The reduction from the naive 10% to the measured 1% is presumably due to a combination of final state interactions, SOS Ytarget acceptance, and missing mass cuts. The Hall C "empty" target consists of two 40 mil thick aluminum windows separated by 4 cm, which can tolerate up to 30 μA. Thus, our "empty" data come in 4 times = (40 mil $\times$ 30 μA) /(4 mil $\times$ 75 μA) faster than window events on the real target. Clearly our empty target measurement overhead will be negligible.

2.6 Anticipated Errors

Based on our E93-021 experience, it is possible to achieve a systematic error on the unseparated $(e,e'\pi)$ cross section of about 3.3%. (Table 6) The SOS acceptance is the largest single contributor, even after limiting ourselves to a 4 cm target and a momentum bite of $\pm$15%. We expect to achieve the same errors in the proposed run. Significantly smaller errors (e.g. 2%) would require restricting the acceptance much further, performing lengthy systematic checks, and more extensive modelling of the experiment. That beam request would be 5 times larger than what we present here. This is not warranted since our projected errors on F_π are well matched to the estimated model dependence. How these systematic errors relate to our projected errors on F_π is now discussed.

To a good approximation in our kinematics, $\sigma_L \propto F_\pi^2$, so we need to first estimate the error on σ_L. Two measurements at fixed (Q^2, W) and different values of ϵ are needed in order to determine σ_L. Thus if

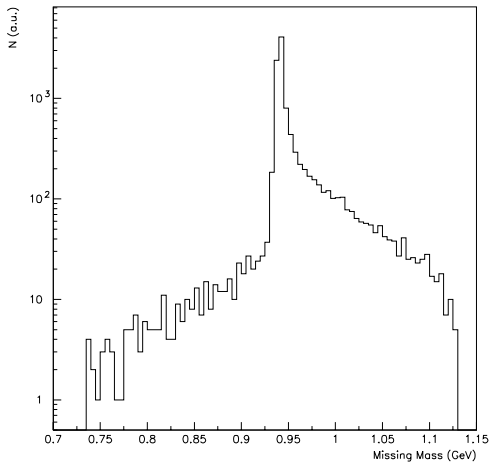

Figure 10: Reconstructed residual neutron mass from E93-021 (log scale). The rms resolution is approximately 1 MeV $\times$ (Ebeam/1GeV). Backgrounds from random coincidences and target windows have been subtracted. Remaining events to the left of the peak are primarily muons from pion decay. To the right of the peak is the radiative tail.

Table 6: Anticipated systematic errors based on our E93-021 experience. The uncorrelated errors between the low and high ϵ settings are given in the last column. The uncorrelated errors dominate the final error on F_π and have been conservatively estimated.

Source	Systematic Errors (%)	Uncorrelated Portion (%)
Acceptance	2.0	2.0
Target Density	1.4	0.5
Radiative Corrections	1.0	1.0
Monte Carlo Generator	1.0	0.5
Charge	0.5	0.5
Tracking	0.5	0.5
Coincidence Blocking	0.5	0.5
Cut Dependence	0.5	0.5
π Decay	1.0	0.0
π Absorption	1.0	0.0
Quadrature Sum	3.3	2.5

Table 7: Projected errors for $F_\pi(Q^2)$ assuming an overall uncorrelated systematic error of 2.5%, the ϵ values given in Table 1, and 30,000 good events per ϵ setting. Model errors are not included. The anticipated error is about 5%, similar to that obtained in E93-021.

Q^2 $(GeV/c)^2$	$r \equiv \sigma_T/\sigma_L$	$\Delta\epsilon$	$\Delta F_\pi/F_\pi$ %
This Proposal			
2.5	0.25	0.26	4.7
2.0	0.30	0.28	5.4
1.6	0.25	0.28	4.7
E93-021 Final Errors			
1.6	0.56	0.35	6.4
1.0	0.33	0.32	5.1
.75	0.43	0.27	7.6
0.6	0.24	0.36	4.5

$\sigma_1 = \sigma_T + \epsilon_1\sigma_L$ and $\sigma_2 = \sigma_T + \epsilon_2\sigma_L$ then

$$\sigma_L = \frac{1}{\epsilon_1 - \epsilon_2}(\sigma_1 - \sigma_2).$$

Assuming uncorrelated errors in the measurement of σ_1 and σ_2, we obtain the intermediate expression

$$\frac{\Delta\sigma_L}{\sigma_L} = \frac{1}{(\epsilon_1 - \epsilon_2)}\frac{1}{\sigma_L}\sqrt{\Delta\sigma_1^2 + \Delta\sigma_2^2}.$$

and by defining $r \equiv \sigma_T/\sigma_L$ and $\Delta\sigma/\sigma \equiv \Delta\sigma_i/\sigma_i$ and assuming $\Delta\sigma_1/\sigma_1 = \Delta\sigma_2/\sigma_2$, then

$$\frac{\Delta\sigma_L}{\sigma_L} = \frac{1}{\epsilon_1 - \epsilon_2}\frac{\Delta\sigma}{\sigma}\sqrt{(r+\epsilon_1)^2 + (r+\epsilon_2)^2}$$

This useful equation makes explicit the error amplification due to a limited ϵ range and (potentially) large r. For the proposed experiment, $r \leq 1$, so a limited ϵ lever arm is our primary source of error amplification, a factor of nearly 4. (Kinematic settings with larger values of $\Delta\epsilon$ are not possible with the HMS-SOS combination at the relatively high value of W where we feel it is important to run this experiment.) Given this significant error amplification for uncorrelated errors, we can virtually ignore *correlated* systematic errors of a few percent. The last column of Table 6 lists only those systematic errors which are likely to be uncorrelated between the low and high ϵ settings. Because low and high epsilon settings are not typically run at similar focal plane rates, rate dependent errors in the table (like tracking efficiencies) are assumed to be uncorrelated. The quadrature sum of the uncorrelated errors is 2.5%. Systematic errors in the kinematic factors (i.e. Γ, Q^2, W^2, and ϵ) are small provided we determine the absolute electron energies to $1 \cdot 10^{-3}$ and the absolute centroids of laboratory scattering angles to 1 mrad.

Again using the approximation that $\sigma_L \propto F_\pi^2$, the experimental error in F_π is

$$\frac{\Delta F_\pi}{F_\pi} = \frac{1}{2}\frac{1}{(\epsilon_1 - \epsilon_2)}\frac{\Delta\sigma}{\sigma}\sqrt{(r+\epsilon_1)^2 + (r+\epsilon_2)^2}.$$

Assuming that 30,000 good events per ϵ setting are used to determine the $-t$ dependence of the reaction (yet another small uncorrelated error), Table 7 gives our anticipated errors for the proposed measurements.[1]

[1] 30,000 events is the total per kinematic setting, but this is divided over 5-6 $|t|$ bins, giving us statistical accuracy of 1.5%, which is a little smaller (as desired) than the our overall uncorrelated systematic error estimate in Table 6 of 2.5%. This will allow the $-t$ dependence of σ_L to be carefully compared to the VGL Regge (or other) model. (See Figure 2.)

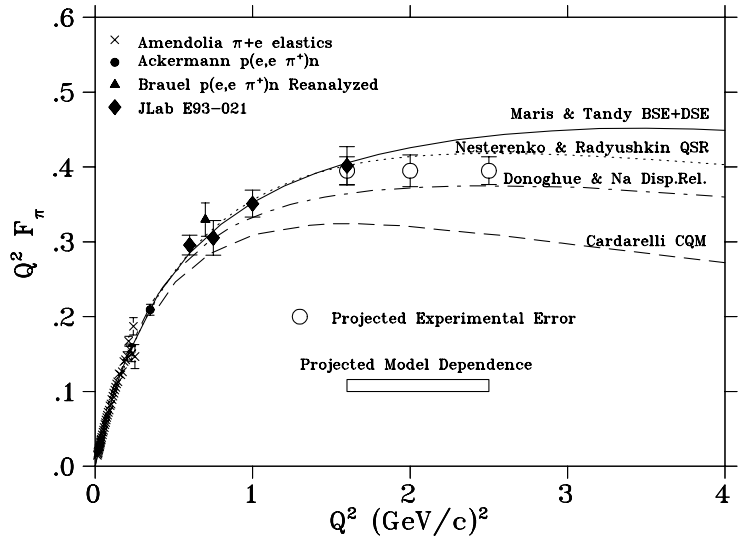

Figure 11: Projected experimental and model errors for this experiment, in comparison with a variety of theoretical models, and high quality existing data, including that of E93-021. The projected model dependence is based on the E93-021 result.

The anticipated error is about 5%, consistent with what was obtained for the most favorable Q^2 settings in E93-021. Because the proposed measurements will be obtained at a higher W than in E93-021, we expect the model uncertainties to be comparable or smaller than those obtained there. Given these caveats, our expected uncertainties are shown in Figure 11.

2.7 Beam Request

The beam request assumes $3{\cdot}10^4$ events per kinematic setting, including detection inefficiencies and cut inefficiencies. (Much of the raw rate for the forward electron angle setting is due to Q^2 and W values which cannot be matched to the smaller phase space of the backward angle setting.) We take the $d(e,e'\pi^+)nn_s$ and $d(e,e'\pi^-)pp_s$ running times to be equal to the $p(e,e'\pi^+)$ time so that accurate values of the separated

Table 8: Beam request for hydrogen and deuterium running. The number of hours per setting is for three $\theta_{\pi q}$ settings at high ϵ and for two $\theta_{\pi q}$ settings at low ϵ (due to the forward angle constraint on the HMS).

Q^2 (GeV/c)^2	W (GeV)	ϵ	LH_2 Hours $p(e,e'\pi^+)$	LD_2 Hours $d(e,e'\pi^+)$	LD_2 Hours $d(e,e'\pi^-)$	Overhead Hours	Total Hours
2.5	2.22	0.540	28	28	28	48	132
		0.277	44	44	44	8	140
2.0	2.22	0.571	12	12	12	24	60
		0.292	32	32	32	8	104
1.6	2.22	0.600	7			24	31
		0.316	30			8	38
Total							505 (21 days)

ratios $\sigma(\pi^-)/\sigma(\pi^+)$ can be obtained. Our overhead assumes 3 shifts to tune each of the three linac gradients required, one shift for each of 6 kinematic settings for angle, target, and momentum changes, and 3 shifts for elastic checkout and sieve slit runs. A summary of the beam request is contained in Table 8.

We request 21 days of beam time to make the proposed measurements at $W = 2.22$ GeV, Q^2=1.6, 2.0 and 2.5 (GeV/c)^2.

3 Closing Statement

Jefferson Lab can make a unique contribution to our knowledge of hadronic structure via the charged pion form factor, F_π. The success of QCD sum rule calculations, constitutent quark models, and Bethe-Salpeter equation approaches can all be tested in the difficult and poorly understood gap between the "soft" and "hard" regions at intermediate Q^2. The pion holds a unique place in this regard, because its $q\bar{q}$ valence structure is relatively simple, and the asymptotic normalization of the wave function is known from $\pi \to \mu\nu$ decay.

E93-021 obtained $\sigma_{\rm L}$ data up to $Q^2 = 1.6$ GeV^2/c^2 in 1997 in Hall C in the kinematical region where the t-pole process is dominant. Values for F_π were extracted from the longitudinal cross section using a recently developed Regge model, and the data globally follow a monopole form obeying the pion charge radius. No other precise data exist above Q^2= 0.7 (GeV/c)^2.

Extending the range of reliable experimental data to higher Q^2 is clearly needed to delineate the role of hard versus soft contributions at intermediate Q^2, and so aid the further development and tests of the QCD-based models currently under development. As indicated in figure 11, the proposed data up to Q^2= 2.5 (GeV/c)^2 will be of sufficient quality to distinguish between at least a number of these models, and so will contribute effectively to our knowledge of hadronic structure.

References

[1] G.R. Farrar, D.R. Jackson, Phys. Rev. Lett. **43** (1979) 246.

[2] R. Jakob, P. Kroll, Phys. Lett. **315B** (1993) 463.

[3] B. Melic, B. Nizic, K. Passek, hep-ph/9908510.

[4] N.G. Stefanis, W. Schroers, H.-Ch. Kim, hep-ph/0005218.

[5] V.M. Braun, A. Khodjamirian, M. Maul, Phys. Rev. D **61** (2000) 073004.

[6] V.A. Nesterenko and A.V. Radyushkin, Phys. Lett **115B** (1982) 410.
A.V. Radyushkin, Nucl. Phys. **A532** (1991) 141.
A.P. Bakulev and A.V. Radyushkin,Phys. Lett. **B271** (1991) 223.

[7] F. Cardarelli et al., Phys. Lett. **332B** (1994) 1.
F. Cardarelli et al., Phys. Lett. **357B** (1995) 267.

[8] H. Ito, W.W. Buck, F. Gross, Phys. Lett. **287B** (1992) 23.

[9] P. Maris, P.C. Tandy, nucl-th/0005015.

[10] N. Isgur, C.H. Llewellyn Smith, Phys. Rev. Lett. **52** (1984) 1080.

[11] S. R. Amendolia *et al.*, Nucl. Phys. **B277** (1986) 168

[12] C. J. Bebek *et al.*, Phys. Rev. D **17** (1978) 1693

[13] H. Ackerman et al., Nucl. Phys. **B137** (1978) 294.

[14] P. Brauel *et al.*, Z. Phys. **C3** (1979) 101

[15] J. Volmer *et al.*, nucl-ex/0010009.

[16] J. Volmer, PhD thesis, Vrije Universiteit, Amsterdam, unpublished

[17] P. E. Bosted, Phys. Rev. C **51** (1995) 409

[18] M. Vanderhaeghen, M. Guidal and J.-M. Laget, Phys. Rev. C **57** (1997) 1454; Nucl. Phys. **A627** (1997) 645

[19] F. Gutbrod and G. Kramer, Nucl. Phys. **B49** (1972) 461

[20] Chen Yan, private communication.

[21] J. O'Connell and J. Lightbody, Comp. in Phys. May-June **57** (1988)
Electron rate: Program QFS, Hadron rates: Program EPC.

[22] J.F Donoghue, E.S. Na, Phys. Rev. D **56** (1997) 7073.